Polarization Dependence of Modal Attraction in High Birefringence Bimodal Optical Fibers

Massimiliano Guasoni and Stefan Wabnitz, *Member, IEEE*

***Abstract*—We study nonlinear mode coupling among two intense and copropagating beams of different wavelength in bimodal and high birefringence optical fibers. With the proper design of the bimodal fiber, we show that this process may lead to modal attraction, where the modal distribution of light at a pump wavelength is replicated at the signal wavelength, independently of the input mode excitation conditions of the signal. We analyse the dependence of the efficiency of the modal attraction process upon the input state of polarization of both the signal and the pump beams.**

***Index Terms*—Fiber nonlinear optics, multiwave mixing, stokes parameters.**

I. Introduction

PROPAGATION in few-mode optical fibers [1] may give rise to a rich variety of nonlinear mode coupling effects [2]–[3]. In particular, all-optical mode switching was theoretically studied and experimentally demonstrated by Pitois *et al.* [4]. In recent years, few mode optical fibers have experienced a resurgency of interest as a transmission medium in coherent high-bit-rate transmission systems via the spatial multiplexing technique [5]–[8].

It is therefore very interesting to further explore the potential of few-mode optical fibers for ultrafast all-optical signal processing devices as well. To this end, we consider here the co-propagation of two beams of arbitrary polarizations and different wavelengths in a bimodal optical fiber. By supposing that at one wavelength the input, say, pump beam is coupled to a mix of the two fiber modes, we show that nonlinear mode coupling may lead to the capability of light to self-organise its modal distribution at the, say, signal wavelength. Namely, a specific point along the fiber exists, where the signal modal distribution is attracted, irrespectively of its input arrangement, to the given input modal distribution of the pump. Because of the analogy with the polarization attraction effect, which occurs in the propagation of two different beams with arbitrary state of polarization (SOP) in a single-mode fiber [9], [10], we may name the present effect as modal attraction.

Manuscript received August 28, 2013; revised November 13, 2013; accepted December 29, 2013. Date of publication January 19, 2014; date of current version February 10, 2014. This work was supported by the European Research Council under Grant 306633, ERC PETAL, and by Fondazione Cariplo, under Grant n.2011-0395.

M. Guasoni is with the Laboratoire Interdisciplinaire Carnot de Bourgogne, UMR 6303 CNRS, Université de Bourgogne, Dijon 21078, France (e-mail: massimiliano.guasoni@u-bourgogne.fr.com).

S. Wabnitz is with the Dipartimento di Ingegneria dell'Informazione, University of Brescia, Brescia 25123, Italy (e-mail: stefan.wabnitz@unibs.it).

Digital Object Identifier 10.1109/JLT.2014.2299755

Modal attraction involving two linearly polarized CW beams which remain aligned with the orthogonal principal axes of a bimodal, high birefringence fiber with elliptical core was recently described in [11]. In this paper, we substantially extend those results by studying the input polarization dependence of the modal attraction process, when considering the most general case where the two input beams have an arbitrary input SOP. As we shall see, for a properly designed double core bimodal optical fiber, involving a depressed index inner core and an elliptical outer core, the effect of modal attraction is still present and highly effective for various input pump and signal SOP configurations.

We first derive in Section II the basic equations ruling nonlinear mode coupling among a pump and a signal of different wavelength and arbitrary SOP in a bimodal, elliptical core fiber. In Section III we discuss the concept of modal attraction and its relationship with the SOP of the interacting modes. In particular, we will point out the special relationship which exists between the property of modal attraction and the choice of the input SOP of the pump and the signal. The strength of modal attraction for some different choices of input polarization configurations is next numerically studied and compared in Section IV. Finally, in Section V we draw our conclusions.

II. Basic Equations

Let us consider an elliptical core fiber which is bimodal in a certain range of wavelengths as determined by its geometrical and physical properties (for details see Section IV). We shall assume that, in the frequency band of bimodality, both x- and y-polarized LP_{01} and $L_{P11,\mathrm{even}}$ modes are supported. Therefore a total of four modes, namely the LP_{01-x}, LP_{01-y}, $LP_{11,\mathrm{even}-x}$ and $L_{P11,\mathrm{even}-y}$ modes, can propagate. For notational simplicity, we shall denote such modes as the $0x$, $0y$, $1x$ and $1y$ mode, respectively. To the contrary, in the considered range of wavelengths the modes $L_{P11,\mathrm{odd}-x}$ and $L_{P11,\mathrm{odd}-y}$ remain below the cut-off frequency, and thus they cannot propagate, so that the fiber is truly bimodal [2]. This special situation permits to study the polarization dependence of modal attraction in a minimal model for a bimodal fiber, and to avoid any possible random coupling among the otherwise nearly degenerate even and odd LP_{11} modes of a circular fiber.

We denote with $U_{nx}(z)$ and $U_{ny}(z)$ the x and y polarized complex amplitudes of modes nx and ny ($n = \{0, 1\}$) at the pump frequency ω_p. Similarly, $V_{nx}(z)$ and $V_{ny}(z)$ denote the mode amplitudes at the signal frequency ω_s. Starting from Maxwell's equations with a polarization which takes into account the nonlinear cubic response of silica, and neglecting all nonlinear terms whose corresponding phase matching (PM)

condition cannot be practically fulfilled, one obtains, by extending equations (8) of [3] to the case of arbitrary polarizations of the coupled waves, the following equations for the evolution of the pump amplitudes with distance z:

$$\begin{aligned} i\frac{dU_{na}}{dz} &= \frac{2}{3}C_{nn}U_{nb}V_{na}V_{nb}^{*}\exp(i\Delta\beta_{1,na}^{(u)}z) \\ &+ \frac{2}{3}C_{01}(3U_{ma}V_{na}V_{ma}^{*}\exp(i\Delta\beta_{2,na}^{(u)}z) \\ &+ U_{mb}V_{na}V_{mb}^{*}\exp(i\Delta\beta_{3,na}^{(u)}z)+U_{nb}V_{ma}V_{mb}^{*}\exp(i\Delta\beta_{4,na}^{(u)}z) \\ &+ U_{nb}U_{ma}U_{mb}^{*}\exp(i\Delta\beta_{5,na}^{(u)}z)+U_{ma}V_{nb}V_{mb}^{*}\exp(i\Delta\beta_{6,na}^{(u)}z)) \\ &+ C_{nn}(|U_{na}|^2+2|V_{na}|^2+\frac{2}{3}(|U_{nb}|^2+|V_{nb}|^2))U_{na} \\ &+ C_{01}(2|U_{ma}|^2+2|V_{ma}|^2+\frac{2}{3}(|U_{mb}|^2+|V_{mb}|^2))U_{na} \end{aligned} \quad (1)$$

where $(n,m)=\{0,1\}, m\neq n$, and $(a,b)=\{x,y\}, a\neq b$. The presence of random linear mode coupling [13] as well as of polarization coupling [8] are both neglected in (1), because of the intrinsic large birefringence induced by the strong core ellipticity, which makes these perturbations to be negligible over a few kilometres (which are the typical fiber lengths involved in our analysis). Equations similar to (1) are obtained for the signal amplitudes V_{na}, by exchanging the labels U and V, and substituting the phase terms $\Delta\beta_{h,\mathrm{na}}^{(u)}$ with $\Delta\beta_{h,\mathrm{na}}^{(v)}$ $(1\leq h\leq 6)$.

The evolution equations for the pump and signal amplitudes permit to extend the study of modal attraction, from the scalar case which was treated in [11], to the general situation where the pump and the signal possess an arbitrary input SOP. In (1) we have set the wave-vector mismatches

$$\begin{aligned} \Delta\beta_{1,na}^{(u)} &= \beta_{nb}(\omega_p)+\beta_{na}(\omega_s)-\beta_{nb}(\omega_s)-\beta_{na}(\omega_p) \\ \Delta\beta_{2,na}^{(u)} &= \beta_{ma}(\omega_p)+\beta_{na}(\omega_s)-\beta_{ma}(\omega_s)-\beta_{na}(\omega_p) \\ \Delta\beta_{3,na}^{(u)} &= \beta_{mb}(\omega_p)+\beta_{na}(\omega_s)-\beta_{mb}(\omega_s)-\beta_{na}(\omega_p) \\ \Delta\beta_{4,na}^{(u)} &= \beta_{nb}(\omega_p)+\beta_{ma}(\omega_s)-\beta_{mb}(\omega_s)-\beta_{na}(\omega_p) \\ \Delta\beta_{5,na}^{(u)} &= \beta_{nb}(\omega_p)+\beta_{ma}(\omega_p)-\beta_{mb}(\omega_p)-\beta_{na}(\omega_p) \\ \Delta\beta_{6,na}^{(u)} &= \beta_{ma}(\omega_p)+\beta_{nb}(\omega_s)-\beta_{mb}(\omega_s)-\beta_{na}(\omega_p). \end{aligned}$$

The mismatches $\Delta\beta_{h,\mathrm{na}}^{(v)}$ are computed by $\Delta\beta_{h,\mathrm{na}}^{(u)}$ by mutual exchanging ω_p and ω_s. Moreover, $\beta_{na}(\omega_f)$ is the propagation constant of mode na at frequency ω_f $(f=\{p,s\})$, $C_{nn}=n_2\omega/(cA_{nn})$ and $C_{01}=n_2\omega/(cA_{01})$ are the fiber nonlinear coefficients, where $n_2=3.2\cdot 10^{-16}\mathrm{cm}^2/\mathrm{W}$ is the silica nonlinear index and c is the speed of light in vacuum. In addition, $A_{nn}=(\int_{xy}|M_n|^2dxdy)^2/(\int_{xy}|M_n|^4dxdy)$ is the intramodal effective area of modes na, and $A_{01}=(\int_{xy}|M_0|^2dxdy)(\int_{xy}|M_1|^2dxdy)/(\int_{xy}|M_0|^2|M_1|^2dxdy)$ is the intermodal effective area involving the LP_{01} and LP_{11} modes, whose modal transverse profiles $M_0(x,y)$ and $M_1(x,y)$ are virtually polarization independent. Under the realistic assumption that $\omega_s\approx\omega_p$, we may set $\omega=(\omega_p+\omega_s)/2$ in the nonlinear coefficients and also consider constant modal profiles as the frequency varies from ω_p to ω_s.

The PM conditions of the oscillating terms read as $|\Delta\beta_{h,\mathrm{na}}^{(u)}|L_{\mathrm{NL}}\ll 1$ and $|\Delta\beta_{h,\mathrm{na}}^{(v)}|L_{\mathrm{NL}}\ll 1$, where $L_{\mathrm{NL}}=1/(C_{00}T)$ is the nonlinear length and $T=(P+S)/2$, P and S being the total powers of the pump and signal wave, respectively. Note that each of the previous PM conditions can be reached in the bimodality band for a proper design of the HiBi fiber. Typically, for a given pump and signal wavelength only a PM condition is fullfilled at a time. Here we restrict our attention to the case where the PM condition $|\Delta\beta_{6,na}^{(u)}|L_{\mathrm{NL}}\ll 1$ is satisfied. This choice allows for a direct comparison with the case that was previously considered in [11], where thanks to the orthogonality between pump and signal, all terms containing $exp(i\Delta\beta_{h,\mathrm{na}}^{(u)}z)$ with $h\leq 5$ vanish in (1). Moreover, we performed extensive finite element simulations showing that the PM condition $|\Delta\beta_{6,na}^{(u)}|L_{\mathrm{NL}}\ll 1$ may indeed be achieved in a relatively large sub-band of the bimodality band while keeping the detuning $\omega_p-\omega_s$ nearly unchanged. Whereas for the other PM conditions the corresponding pump-signal detuning is strictly dependent on the choice of the pump wavelength.

From the previously given definition of the wave vectors mismatches, it is straightforward to obtain the relations $\Delta\beta_{6,0x}^{(u)}=\Delta\beta_{6,1y}^{(v)}=-\Delta\beta_{6,1x}^{(u)}=-\Delta\beta_{6,0y}^{(v)}$ and $\Delta\beta_{6,0y}^{(u)}=\Delta\beta_{6,1x}^{(v)}=-\Delta\beta_{6,1y}^{(u)}=-\Delta\beta_{6,0x}^{(v)}$. Therefore there are only two independent wave vectors, which we denote as $\mathrm{PM}'=\{\Delta\beta_{6,0x}^{(u)},-\Delta\beta_{6,1x}^{(u)},-\Delta\beta_{6,0y}^{(v)},\Delta\beta_{6,1y}^{(v)}\}$ and $\mathrm{PM}''=\{\Delta\beta_{6,0y}^{(u)},-\Delta\beta_{6,1y}^{(u)},-\Delta\beta_{6,0x}^{(v)},\Delta\beta_{6,1x}^{(v)}\}$. Alternatively, the two independent wave vectors in (1) may be simply represented by $\Delta\beta_{6,0x}^{(u)}$ and $\Delta\beta_{6,0y}^{(u)}$, respectively.

In practice, the two PM conditions $|\Delta\beta_{6,0x}^{(u)}|L_{\mathrm{NL}}\ll 1$ and $|\Delta\beta_{6,0y}^{(u)}|L_{\mathrm{NL}}\ll 1$ cannot be achieved at the same time. Moreover, in the presence of phase mismatch among the interacting modes, i.e., $|\Delta\beta_{6,0x}^{(u)}|L_{\mathrm{NL}}\gg 1$ and $|\Delta\beta_{6,0y}^{(u)}|L_{\mathrm{NL}}\gg 1$, there are no modal energy exchanges and all modal amplitudes are conserved, i.e., $d|V_{na}|^2/dz=d|U_{na}|^2/dz=0$.

Hereafter we shall focus our attention to the case $|\Delta\beta_{6,0x}^{(u)}|L_{\mathrm{NL}}\ll 1$ and $|\Delta\beta_{6,0y}^{(u)}|L_{\mathrm{NL}}\gg 1$. These conditions, which can be achieved in practice by means of a proper design of the bimodal fiber (see Section IV), do enable the transfer of energy among the fiber modes.

In a manner similar to what it was done in [11], we introduce here the modal Stokes vectors $\mathbf{P_x},\mathbf{P_y},\mathbf{S_x},\mathbf{S_y}$, in analogy with the polarization Stokes vectors that are used for describing the light SOP. The vector $\mathbf{P_a}=[P_{a1},P_{a2},P_{a3}]^T$ $(a=\{x,y\})$ has components $P_{a1}=U_{0a}U_{1a}^{*}+U_{1a}U_{0a}^{*}$, $P_{a2}=-iU_{0a}U_{1a}^{*}+iU_{1a}U_{0a}^{*}$, $P_{a3}=|U_{0a}|^2-|U_{1a}|^2$, respectively. The components of the vector $\mathbf{S_a}=[S_{a1},S_{a2},S_{a3}]^T$ are similarly defined, after exchanging the labels U and V. Both $\mathbf{P_a}$ and $\mathbf{S_a}$ conserve their magnitude $P_{a0}=(P_{a1}^2+P_{a2}^2+P_{a3}^2)^{1/2}=|U_{0a}|^2+|U_{1a}|^2$ and $S_{a0}=(S_{a1}^2+S_{a2}^2+S_{a3}^2)^{1/2}=|V_{0a}|^2+|V_{1a}|^2$. The normalized vectors $\bar{\mathbf{P}}_\mathbf{a}=\mathbf{P_a}/P_{a0}$ and $\bar{\mathbf{S}}_\mathbf{a}=\mathbf{S_a}/S_{a0}$ are referred to as the unitary modal Stokes vectors.

Under the conditions $|\Delta\beta^{(u)}_{6,0x}|L_{\rm NL} \ll 1$ and $|\Delta\beta^{(u)}_{6,0y}|L_{\rm NL} \gg 1$, and using the previous definitions of modal Stokes vectors, Equation (1) may be recast as follows

$$\frac{d\mathbf{P_x}}{dz} = C_A\mathbf{P_x}\times I_1\mathbf{P_x} + 2C_B\mathbf{P_x}\times I_1\mathbf{S_x} + \frac{2}{3}C_B\mathbf{P_x} \times I_1\mathbf{P_y} + \frac{2}{3}C_B\mathbf{P_x}\times I_1\mathbf{S_y} + C_{px,1}\mathbf{P_x}\times I_1\mathbf{U} + C_{px,2}\mathbf{P_x}\times I_2\mathbf{S_y} \quad (2)$$

$$\frac{d\mathbf{S_y}}{dz} = C_A\mathbf{S_y}\times I_1\mathbf{S_y} + 2C_B\mathbf{S_y}\times I_1\mathbf{P_y} + \frac{2}{3}C_B\mathbf{S_y} \times I_1\mathbf{S_x} + \frac{2}{3}C_B\mathbf{S_y}\times I_1\mathbf{P_x} + C_{sy,1}\mathbf{S_y}\times I_1\mathbf{U} + C_{sy,2}\mathbf{S_y}\times I_2\mathbf{P_x} \quad (3)$$

where $C_A = 2C_{01} - (C_{00}+C_{11})/2$; $C_B = C_{01} - (C_{00}+C_{11})/2$; $C_{px,1} = (1/2)(C_{11}-C_{00})(P_{x0}+2S_{x0}+(2/3)P_{y0}+(2/3)S_{y0})$; $C_{sy,1} = (1/2)(C_{11}-C_{00})(S_{y0}+2P_{y0}+(2/3)S_{x0}+(2/3)P_{x0})$; $C_{px,2} = C_{sy,2} = -(2/3)C_{01}$; $I_1 = \mathrm{diag}(0,0,1)$; $I_2 = \mathrm{diag}(1,1,0)$; $\mathbf{U} = [0,0,1]^T$. Similar equations are obtained for $\mathbf{P}_y$ and $\mathbf{S}_x$ after interchanging x and y labels in (2), (3), and by setting $C_{py,2} = C_{sx,2} = 0$. Therefore (2), (3), along with their associated equations for $\mathbf{P}_y$ and $\mathbf{S}_x$, provide a closed system of four coupled nonlinear evolution equations for the modal Stokes vectors.

As it was discussed in [11], the components $\bar{P}_{a3}(z)$ and $\bar{S}_{a3}(z)$ describe the relative modal power distribution (MPD) among the two $a-$ polarized modes at the pump and signal wavelengths, respectively. Under the assumption that $|\Delta\beta^{(u)}_{6,0x}|L_{\rm NL} \ll 1$ and $|\Delta\beta^{(u)}_{6,0y}|L_{\rm NL} \gg 1$, the mode amplitudes $|U_{0y}|^2, |U_{1y}|^2, |V_{0x}|^2$ and $|V_{1x}|^2$ are conserved upon propagation, altogether with the y-pump MPD $\bar{P}_{y3}$ and the x-signal MPD $\bar{S}_{x3}$. On the other hand, the pump x-MPD $\bar{P}_{x3}$ and the signal y-MPD $\bar{S}_{y3}$ are allowed to vary along the fiber. It turns out that, with a proper choice of the fiber nonlinear coupling coefficients, the input pump x-MPD $\bar{P}_{x3}(0)$ may be replicated by the signal y-MPD $\bar{S}_{y3}(L)$ at a peculiar position, say, $z = L$ along the fiber. This occurs virtually irrespectively of the specific input value of the y-MPD $\bar{S}_{y3}(0)$. Such effect was introduced in [11] for the particular case where pump and signal remain orthogonally polarized along the principal axes of the fiber, and it was named modal attraction. In Section III we shall provide a detailed discussion of modal attraction, for the general case where the pump and signal beams may have an arbitrary SOP.

We would like to point out here that all results for the case with $|\Delta\beta^{(u)}_{6,0x}|L_{\rm NL} \ll 1$ and $|\Delta\beta^{(u)}_{6,0y}|L_{\rm NL} \gg 1$ also apply to the situations where $|\Delta\beta^{(u)}_{6,0x}|L_{\rm NL} \gg 1$ and $|\Delta\beta^{(u)}_{6,0y}|L_{\rm NL} \ll 1$, providing that $\mathbf{P_x}$ is exchanged with $\mathbf{P_y}$, and $\mathbf{S_x}$ with $\mathbf{S_y}$. Therefore it is sufficient to limit our discussion to the former case.

III. Modal Attraction

As previously outlined, the concept of modal attraction means that, at a certain distance L along the fiber, one obtains that $\bar{S}_{y3}(L) \to \bar{P}_{x3}(0)$, irrespectively of the input signal MPD $\bar{S}_{y3}(0)$. Attention should be paid to the fact that the input vectors $\bar{\mathbf{S}}_{\mathbf{x}}(0)$ and $\bar{\mathbf{S}}_{\mathbf{y}}(0)$ are not independent, as the equality $\bar{\mathbf{S}}_{\mathbf{x}}(0) = \bar{\mathbf{S}}_{\mathbf{y}}(0)$ holds true (see Appendix). Similarly, $\bar{\mathbf{P}}_{\mathbf{x}}(0) = \bar{\mathbf{P}}_{\mathbf{y}}(0)$. Moreover, the system of (2), (3) (and the associated equations for $\mathbf{P}_y$ and $\mathbf{S}_x$) turns out to be invariant with respect to rotations of the input modal Stokes vectors about the third (i.e. P_{a3} and S_{a3}) modal axis. That is, any rotation of the input values $\bar{\mathbf{P}}_{\mathbf{x}}(0) \equiv \bar{\mathbf{P}}_{\mathbf{y}}(0)$ and $\bar{\mathbf{S}}_{\mathbf{x}}(0) \equiv \bar{\mathbf{S}}_{\mathbf{y}}(0)$ about the respective third modal axis simply leads to the same rotation of the output modal Stokes vectors, namely of $\bar{\mathbf{P}}_{\mathbf{x}}(z), \bar{\mathbf{P}}_{\mathbf{y}}(z), \bar{\mathbf{S}}_{\mathbf{x}}(z)$ and $\bar{\mathbf{S}}_{\mathbf{y}}(z)$. Without any loss of generality, this permits us to fix $\bar{P}_{x2}(0) \equiv \bar{P}_{y2}(0) = 0$ and $\bar{P}_{x1}(0) \equiv \bar{P}_{y1}(0) \geq 0$, so that the vectors $\bar{\mathbf{P}}_{\mathbf{x}}(0)$ and $\bar{\mathbf{P}}_{\mathbf{y}}(0)$ lie over the semicircle $S_2 = 0, S_1 > 0$ of the modal Poincaré sphere (see Fig. 2, where $S_{1,2,3}$ identify the three axes of the sphere), and are fully specified by the value of $\bar{P}_{x3}(0) \equiv \bar{P}_{y3}(0)$.

Once that the pump and signal powers P_{a0} and S_{a0} (with $a = \{x, y\}$) as well as the input pump MPD $\bar{P}_{x3}(0) \equiv \bar{P}_{y3}(0)$ are fixed, we may quantify the attraction strength by solving the system of (2), (3) (and the associated equations for $\mathbf{P}_y$ and $\mathbf{S}_x$) for a set of N different input unitary modal Stokes vectors $\bar{\mathbf{S}}^{(k)}_{\mathbf{x}}(0) \equiv \bar{\mathbf{S}}^{(k)}_{\mathbf{y}}(0)$ $(1 \leq k \leq N)$ which are uniformly distributed over the modal Poincaré sphere. Next we may evaluate the average of the signal y-MPD $\mu(z) = \langle \bar{S}^{(k)}_{y3}(z)\rangle$ over the ensemble of all modal input Stokes vectors, along with its standard deviation $\sigma(z) = (\langle \bar{S}^{(k)}_{y3}(z)^2 - \mu(z)^2\rangle)^{1/2}$. Finally, the degree of modal attraction (DOMA) is computed as $\mathrm{DOMA}(z) = 1 - \sqrt{3}\sigma(z)$. The upper bound DOMA=1 is reached whenever full modal attraction is achieved, whereas the lower bound DOMA$=1-\sqrt{3}$ corresponds to the case where the instances $\bar{S}^{(k)}_{y3}$ take the values ± 1 with an equal probability. A DOMA=0 corresponds instead to the case where the instances $\bar{S}^{(k)}_{y3}$ are uniformly distributed between -1 and 1, i.e. when modal attraction is absent [11].

The evolution of the third component of the unitary modal Stokes vector, $\bar{S}^{(k)}_{y3}(z)$, turns out to be periodic along the fiber. As it was discussed in [11], the modal attraction process is based on the possibility of obtaining, provided that a proper choice of the nonlinear coupling coefficients is made, that the period of evolution of any trajectory $\bar{S}^{(k)}_{y3}(z)$ remains nearly independent of its input value $\bar{S}^{(k)}_{y3}(0)$. Under such condition, it is possible to find a particular point $z = L$ along the fiber such that all istances $\bar{S}^{(k)}_{y3}(L)$ coalesce to one and the same value [11]. Note that such attraction property does not hold for the other components $\bar{S}_{y1}(z)$ and $\bar{S}_{y2}(z)$. Hence this justifies our definition of DOMA which only involves the third component of the modal Stokes vectors.

Numerical simulations, such as those described in the next Section IV, reveal that the efficiency of the modal attraction grows larger whenever the phase difference ϕ_s between the input signal modal amplitudes $V_{0a}(0)$ and $V_{1a}(0)$ is equal to the phase difference ϕ_p between the input pump modal amplitudes $U_{0a}(0)$ and $U_{1a}(0)$. We shall refer to this situation as the condition of in-phase input modal excitation. By supposing that $\bar{P}_{x2}(0) \equiv \bar{P}_{y2}(0) = 0$ and $\bar{P}_{x1}(0) \equiv \bar{P}_{y1}(0) \geq 0$, the condition of in-phase input modal excitation means that $\bar{S}_{x2}(0) \equiv$

$\bar{S}_{y2}(0) = 0$ and $\bar{S}_{x1}(0) \equiv \bar{S}_{y1}(0) \geq 0$. Otherwise we shall say that the input modal excitation is not in-phase, a situation which may considerably reduce the strength of the attraction process.

The main objective of this paper is to show that there is an additional factor which strongly affects the modal attraction process, namely the choice of the input signal and pump SOPs. We will denote the polarization Stokes vectors with lower case in order to distinguish them from the modal Stokes vectors that we indicate with capital letters. The pump SOP coupled to the mode LP_{n1} $(n = \{0, 1\})$ is described by the dimensionless polarization Stokes vector $\mathbf{p_n} = [p_{n1}, p_{n2}, p_{n3}]$, whose components are $p_{n1} = (U_{nx}U_{ny}^* + U_{nx}^*U_{ny})/p_{n0}$, $p_{n2} = (-iU_{nx}U_{ny}^* + iU_{nx}^*U_{ny})/p_{n0}$, $p_{n3} = (|U_{nx}|^2 - |U_{ny}|^2)/p_{n0}$ and where $p_{n0} = |U_{nx}|^2 + |U_{ny}|^2$; the signal SOP is described by the Stokes vector $\mathbf{s_n} = [s_{n1}, s_{n2}, s_{n3}]$ which is obtained with the same definitions that we used for the pump, after exchanging the U and V labels. Similarly to the case of the input unitary modal Stokes vectors, the input SOPs of the pump and the signal are linked by the constraints $\mathbf{p_0}(0) = \mathbf{p_1}(0)$ and $\mathbf{s_0}(0) = \mathbf{s_1}(0)$ (see Appendix).

We highlight that both the modal and the polarization Stokes vectors that we use in this study are either components or linear combination of components of the generalized Stokes vector which was introduced in [12] in the frame of the modal dispersion analysis of multimode fibers.

Note that the input modal Stokes vectors may be univocally determined once that the modal powers p_{n0} and s_{n0} and the relative phase $\Delta\phi = \phi_p - \phi_s$, as well as the input SOPs of pump and signal are known. More precisely, the input modal Stokes vectors turn out to depend only on the third components $v_p = p_{n3}(0)$ and $v_s = s_{n3}(0)$ of the input SOPs. As a consequence, the output values of the DOMA are independent of the particular choice of $p_{n1}(0)$, $p_{n2}(0)$, $s_{n1}(0)$ and $s_{n2}(0)$. The following relations hold (see Appendix): $\mathbf{P_x}(0) = (P/2)(1 + v_p)\bar{\mathbf{P}}(0)$, $\mathbf{P_y}(0) = (P/2)(1 - v_p)\bar{\mathbf{P}}(0)$, $\mathbf{S_x}(0) = (S/2)(1 + v_s)\bar{\mathbf{S}}(0)$ and $\mathbf{S_y}(0) = (S/2)(1 - v_s)\bar{\mathbf{S}}(0)$, where $\bar{\mathbf{P}}(0) = \bar{\mathbf{P}}_\mathbf{x}(0) = \bar{\mathbf{P}}_\mathbf{y}(0) = [\alpha_p, 0, \nu_p]$ and $\bar{\mathbf{S}}(0) = \bar{\mathbf{S}}_\mathbf{x}(0) = \bar{\mathbf{S}}_\mathbf{y}(0) = [\alpha_s \cos(\Delta\phi), \alpha_s \sin(\Delta\phi), \nu_s]$, with $\alpha_p = 2(p_{00}(0)\, p_{10}(0))^{1/2}/P$, $\nu_p = (p_{00}(0) - p_{10}(0))/P$, and $P = p_{00}(0) + p_{10}(0)$ is the conserved total pump power. Moreover, α_s, ν_s are obtained as α_p, ν_p after exchanging $\{P, p\}$ and $\{S, s\}$ labels.

Whenever the modal powers and $\Delta\phi$ are fixed, different values of v_p and v_s generally lead to a different strengths of modal attraction. Here, to put in evidence the polarization dependence of the modal attraction, we shall focus on three particular polarization arrangements. In the first configuration, both pump and signal exhibit an input elliptical SOP of the type $\mathbf{p_0}(0) \equiv \mathbf{p_1}(0) = [p, q, 0]$ and $\mathbf{s_0}(0) \equiv \mathbf{s_1}(0) = [s, t, 0]$ (so that $v_p = v_s = 0$). In the second case, the input signal SOP is elliptical ($\mathbf{s_0}(0) \equiv \mathbf{s_1}(0) = [s, t, 0]$), while the input pump SOP is linear and its orientation is aligned with a principal axis of the birefringent fiber, namely, $\mathbf{p_0}(0) \equiv \mathbf{p_1}(0) = [0, 0, \pm 1]$ (so that $v_s = 0$, and $v_p = \pm 1$). Finally, the third input polarization arrangement is obtained in the same way as the second arrangement, after interchanging the pump and signal SOPs (i.e., with $\mathbf{s_0}(0) \equiv \mathbf{s_1}(0) = [0, 0, \pm 1]$ and $\mathbf{p_0}(0) \equiv \mathbf{p_1}(0) = [p, q, 0]$), so that $v_s = \pm 1$, and $v_p = 0$).

As we shall see in the next Section IV, in spite of the fact that with the previously described input polarization arrangements the DOMA does not depend on the particular values of p, q, s, t, yet each arrangement exhibits its own specific modal attraction properties. Moreover, in Section IV we will also compare the modal attraction properties of these three input SOP configurations with a special fourth configuration where pump and signal are orthogonally polarized along the two principal axes of the fiber, i.e. $\mathbf{p_0}(0) \equiv \mathbf{p_1}(0) = [0, 0, \pm 1]$ and $\mathbf{s_0}(0) \equiv \mathbf{s_1}(0) = [0, 0, \mp 1]$ $(v_s = \mp, v_p = \pm 1)$. This last case was previously analyzed in [11], and it turns out to yield the highest DOMA values.

IV. Numerical Results

The numerical simulations of (2), (3) (and the associated equations for $\mathbf{P}_y$ and $\mathbf{S}_x$) that we will present in this Section will show that the efficiency of modal attraction not only depends upon the input SOP and relative phase $\Delta\phi$, but it is also strongly affected by the ratio between pump and signal power, as well as by the magnitude of the nonlinear coupling coefficients.

Indeed, a threshold value, say, C of the coefficient C_{01} exists, such that efficient modal attraction requires that $C_{01} \geq C$. Otherwise, whenever $C_{01} < C$ it turns out that the period and the range of oscillations of the parameter $\bar{S}_{y3}^{(k)}(z)$ vary with the input Stokes modal parameter $\bar{S}_{y3}^{(k)}(0)$, so that there is no unique coalescence point L for all of the corresponding individual modal parameter evolutions [11].

As consequence, if $C_{01} < C$ the DOMA remains at relatively low levels. To the contrary, whenever $C_{01} > C$ it turns out that it is possible to find a single merging point $z = L$ for all of the modal parameter evolutions. Therefore at precisely $z = L$ the DOMA is close to the unit value. The critical coupling C strictly depends on the third components p_{n3} and s_{n3} of the input signal and pump SOP, therefore the actual values of C are quite different in each of the four input polarization arrangements that we presented in the previous Section III. In each case, the critical coupling value C is defined as the minimum value of the coefficient C_{01} that still allows for a peak DOMA which is larger than 0.8 whenever the following conditions are verified: 1) P = S, 2) in-phase input modal excitation, and 3) $\bar{P}_{x3}(0) \equiv \bar{P}_{y3}(0) = 0$ (which is the input pump MPD that provides the most efficient modal attraction).

Whenever the pump and the signal are orthogonally polarized, and aligned with the two principal axes of the birefringent bimodal fiber, one obtains that $C \approx 0.15 \max(C_{00}, C_{11})$. Such value of the critical coupling coefficient C is much lower than the corresponding values which are obtained in the other three input polarization arrangements that we discussed in Section III. Indeed, in those configurations one obtains that it is necessary to have $C = C_{01} \approx 0.7 \max(C_{00}, C_{11})$ for obtaining an efficient modal attraction. We performed numerical finite element simulations using the COMSOL software, and found that such an high value of C_{01} is not achievable in bimodal elliptical step-index fibers, where typically $C_{01} < 0.5 \max(C_{00}, C_{11})$. On the other hand, the condition $C = C_{01} \approx 0.7 \max(C_{00}, C_{11})$ may be obtained by using a depressed index core fiber, such as the one

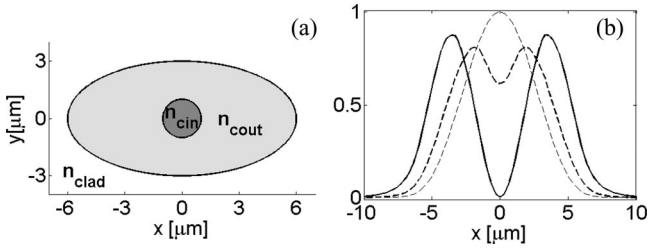

Fig. 1. Panel (a) illustrates the cross-section of the depressed index core bimodal high birefringence fiber. In light-gray we show the outer elliptical core of refractive index $n_{\rm cout} = 1.45$ and radii $R_{x\rm out} = 5.60\mu$m and $R_{y\rm out} = 2.80\mu$m; in dark-gray we show the inner circular core of index $n_{\rm cin} = 1.44$ and radius $R_{\rm in} = 0.95\mu$m. Panel (b) shows the profile of the fiber modes in the slice $y = 0$: the bold dashed curve shows the LP_{01} ($M_0(x, y = 0)$) mode; the thin dashed curve shows the LP_{01} mode obtained with a step-index fiber without index depression ($n_{\rm cin} = n_{\rm cout} = 1.45$); the bold solid curve shows the $LP_{11,\rm even}$ ($M_1(x, y = 0)$) mode which remains virtually unchanged in both the depressed index core geometry and in the step-index fiber. Note that in the depressed index geometry the LP_{01} mode penetrates further in the high-index outer core than in the step-index case.

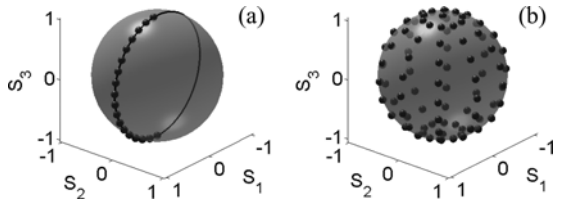

Fig. 2. Input distribution of the vectors $\bar{\mathbf{S}}_{\mathbf{y}}^{(k)}(0)$ over the modal Poincaré sphere. In (a): the tips of the vectors are situated over the semicircle $S_2 = 0, S_1 > 0$ (in-phase input modal excitation); in (b): the tips of the input vectors uniformly cover the whole sphere (the input modal excitation is not in-phase). The black solid curve in (a) represents the meridian $S_2 = 0$.

whose cross-section is depicted in Fig. 1(a). This fiber is composed by a cladding of index $n_{\rm clad} = 1.44$, and a double core which includes an inner circular core with index $n_{\rm cin} = 1.44$ and an outer elliptical core with index $n_{\rm cout} = 1.45$, respectively. The two radii of the outer core are $R_{x\rm out} = 5.60\,\mu$m and $R_{y\rm out} = 2.80\,\mu$m, whereas the inner core radius is $R_{\rm in} = 0.95\,\mu$m.

Note that the lower $n_{\rm cin}$ with respect to $n_{\rm cout}$, the higher is the spreading of the LP_{01} modes out of the inner core into the higher-index, outer elliptical core. On the other hand, the LP_{11} modes are substantially unaffected by changes of the difference $n_{\rm cin} - n_{\rm cout}$ [see Fig. 1(b)]. This fact allows for increasing the overlap integral $\int_{xy} |M_0|^2 |M_1|^2 \partial x \partial y$, hence the coefficient C_{01}, with respect to the step-index fiber case (i.e., the same fiber as in Fig. 1(a), but with $n_{\rm cin} = n_{\rm cout} = 1.45$). The depressed index core fiber of Fig. 1(a) is bimodal over the telecom band from 1520 nm to 1580 nm, where the PM condition $|\Delta\beta_{6,0x}^{(u)}| L_{\rm NL} \ll 1$ is verified for a pump-signal wavelength separation of about 10 nm. Moreover, the nonlinear coefficients satisfy the relations $C_{01} \approx 0.75 C_{00}$, $C_{00} \approx C_{11}$. At the center of the C band (e.g., for a pump at 1550 nm, and a signal at 1560 nm) one obtains $C_{01} = 1.41\ \text{km}^{-1}\text{W}^{-1}$ and $C_{00} = C_{11} = 1.89\ \text{km}^{-1}\text{W}^{-1}$, which represent typical values for the nonlinear coefficient of standard silica fibers.

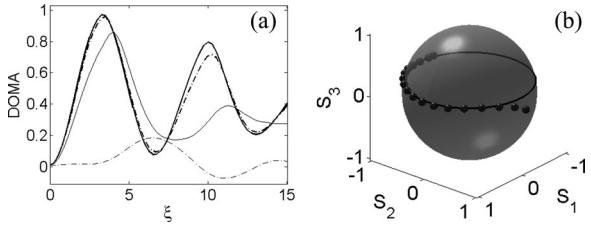

Fig. 3. Panel (a): DOMA versus dimensionless distance ξ when pump and signal are linearly polarized and aligned with the x- and y-axes, respectively, $P_{x0} = S_{y0}$, for in-phase input modal excitation. Results are shown for different input pump MPDs: $\bar{P}_{x3}(0) = 0$ (bold line); $\bar{P}_{x3}(0) = \pm 0.2$(bold dashed-dot line); $\bar{P}_{x3}(0) = \pm 0.6$ (thin line); $\bar{P}_{x3}(0) = \pm 0.99$(thin dashed-dot line). Panel (b) depicts the tips of the output vectors $\bar{\mathbf{S}}_{\mathbf{y}}^{(k)}(\xi = 3.5)$ for an input pump MPD $\bar{P}_{x3}(0) = 0.2$, showing their distribution along the parallel $S_3 = 0.2$ (black line).

Fig. 3 illustrates the spatial evolution of the DOMA along the fiber, for the special case where pump and signal are orthogonally polarized, and aligned with the x and y axes of the fiber, respectively ($P_{y0} = S_{x0} = 0$). Here the nonlinear coupling coefficients correspond to the depressed index core fiber shown in Fig. 1(a), i.e., $C_{01} \approx 0.75 C_{00}$ and $C_{00} \approx C_{11}$. Hereafter we shall consider the dimensionless distance $\xi \equiv z/L_s$, where $L_s = 1/(C_{00} S)$ and $S = S_{x0} + S_{y0}$ is the total signal power. As previously noted, without loss of generality we may also set $\bar{P}_{x2}(0) = 0$ and $\bar{P}_{x1}(0) > 0$. The results which are shown in Fig. 3(a) involve in-phase modal excitation, and equal power pumps and signals ($P_{x0} = S_{y0}$). The ensemble of the $N = 100$ input vectors $\bar{\mathbf{S}}_{\mathbf{y}}^{(k)}(0)$ ($1 \le k \le 100$) was chosen so that their tips are located on the semicircle of the modal Poincaré sphere which is defined by the conditions $S_2 = 0, S_1 > 0$ [Fig. 2(a)]. As it can be seen, nearly unitary DOMA values are reached for almost all input pump MPDs, except for the case with $\bar{P}_{x3}(0) \to 1$ (or $\bar{P}_{x3}(0) \to -1$), i.e., whenever nearly all of the pump is coupled to the mode $0x$ (or the mode $1x$).

Fig. 3 reveals a general property of modal attraction, namely that the point $\xi_{\rm peak}$ along the fiber where a peak value of DOMA is reached is nearly the same for all input pump MPD values. In Fig. 3 one has that $\xi_{\rm peak} \approx 3.5$ for what we may call the modal attraction point. In real units, for $S_{y0} = 1\,W$ and $C_{00} = 1.89\ \text{km}^{-1}\text{W}^{-1}$, $\xi_{\rm peak} \approx 3.5$ corresponds to $z_{\rm peak} = 1.85$ km. The strength of modal attraction is well illustrated in Fig. 3(b), where we show the distribution of the output vectors $\bar{\mathbf{S}}_{\mathbf{y}}^{(k)}(\xi_{\rm peak})$ on the modal Poincaré sphere for $\bar{P}_{x3}(0) = 0.2$. In this case the DOMA $= 0.97$: Fig. 3(b) shows that all vectors $\bar{\mathbf{S}}_{\mathbf{y}}^{(k)}(\xi_{\rm peak})$ remain in the range 0.17 and 0.22, i.e., within a narrow ring centered around the parallel $S_3 = \bar{P}_{x3}(0) = 0.2$. The nearly unitary value of DOMA means that $\bar{S}_{y3}^{(k)}(\xi_{\rm peak}) \to \bar{P}_{x3}(0)$.

Whenever out-of-phase input modal excitation is used, a strong reduction of DOMA results, as it can be seen in Fig. 4(a): here we show the DOMA evolutions which are obtained whenever the N=1000 input tips $\bar{\mathbf{S}}_{\mathbf{y}}^{(k)}(0)$ uniformly cover the modal Poincaré sphere [see Fig. 2(b)], so that the corresponding relative phases $\Delta\phi^{(k)}$ are uniformly distributed between $-\pi$ and π. In this case, the maximum DOMA$= 0.37$. Therefore, in the

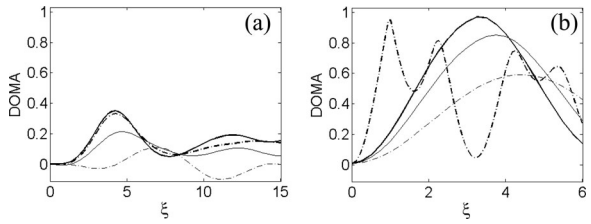

Fig. 4. In (a): same as in Fig. 3(a), for out-of-phase input modal excitation. Panel (b): DOMA versus ξ when pump and signal are linearly polarized and aligned with the x- and y-axes, respectively, $\bar{P}_{x3}(0) = 0$ and for in-phase input modal excitation. Results are shown for different ratios $r = P/S$: r = 0.5 (thin dashed-dot line); r = 0.8 (thin line); r = 1 (bold line); r = 3 (bold dashed-dot line).

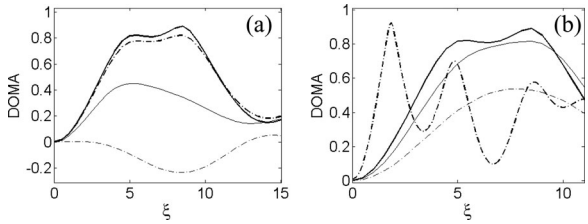

Fig. 5. Panel (a) shows the DOMA versus ξ when both pump and signal have input elliptical polarization ($\mathbf{p_0}(0) \equiv \mathbf{p_1}(0) = [p, q, 0]$ and $\mathbf{s_0}(0) \equiv \mathbf{s_1}(0) = [s, t, 0]$), $P_{x0} = S_{y0}$, for in-phase input modal excitation. Results are shown for different input pump MPDs: $\bar{P}_{x3}(0) = 0$ (bold line); $\bar{P}_{x3}(0) = \pm 0.2$ (bold dashed-dot line); $\bar{P}_{x3}(0) = \pm 0.6$ (thin line); $\bar{P}_{x3}(0) = \pm 0.99$ (thin dashed-dot line). Panel (b) shows the DOMA versus ξ when pump and signal have an input elliptical polarization, $\bar{P}_{x3}(0) = 0$, for in-phase input modal excitation. Results are shown for different ratios $r = P/S$: r = 0.5(thin dashed-dot line); $r = 0.8$ (thin line); $r = 1$ (bold line); $r = 3$ (bold dashed-dot line).

present case in-phase input modal excitation is a mandatory condition for achieving DOMA values close to one.

Indeed our simulations indicate that, in the out-of-phase situation, the DOMA never approaches unity. Nevertheless, it turns out that by changing the values of the nonlinear coefficients in (2), (3), relatively large DOMA values may still be obtained for some specific polarization arrangements of the pump and signal. Compare for example Fig. 4(a) with the result presented in Fig. 2(b) of [11], where $C_{01} \approx 0.2C_{00}$, $C_{11} \approx 0.16C_{00}$, and a peak DOMA $= 0.65$ was reported. In general, in the out-of-phase situation DOMA values up to 0.7 may still be achieved whenever $C_{01} \ll \max(C_{00}, C_{11})$, but only provided that the pump and signal are orthogonal and linearly polarized with the linear birefringence axes. Moreover, such cases involve a significant increase of the peak DOMA position ξ_{peak}, i.e., of the necessary fiber length. E.g., in Fig. 4(a) we have $\xi_{\mathrm{peak}} = 4$, whereas $\xi_{\mathrm{peak}} = 26$ in Fig. 2(b) of [11].

Another parameter which deeply affects the strength of modal attraction is the ratio $r = P/S$ between the total pump and signal power. In Fig. 4(b) we show the DOMA evolution with distance ξ for different values of r, with $\bar{P}_{x3}(0) = 0$ and in-phase input modal excitation. As it can be seen, the condition for the DOMA to reach high values is that the pump power is nearly equal or larger than the signal power ($r > 0.8$). Otherwise, when for example $r = 0.5$, the peak DOMA is reduced down to 0.59.

Let us turn our attention now to the first input polarization arrangement that we discussed in Section III, involving a pump and a signal with input elliptical SOP of the type $\mathbf{p_0}(0) \equiv \mathbf{p_1}(0) = [p, q, 0]$ and $\mathbf{s_0}(0) \equiv \mathbf{s_1}(0) = [s, t, 0]$. In such input configuration, one obtains the DOMA evolutions which are reported in Fig. 5: here panel (a) corresponds to in-phase input modal excitation and $P_{x0} = S_{y0}$ (note that $P_{x0} = P_{y0}$ and $S_{x0} = S_{y0}$). As it can be seen, a peak value of DOMA=0.89 is obtained at the distance $\xi = 8.5$ whenever $\bar{P}_{x3}(0) \equiv \bar{P}_{y3}(0) = 0$. We may thus conclude that, with this input polarization arrangement, the maximum value of the DOMA is reduced, and it is obtained at a longer distance, with respect to the previously considered case of linearly polarized and orthogonal pump and signal. In any case, modal attraction remains quite efficient whenever $-0.4 < \bar{P}_{x3}(0) \equiv \bar{P}_{y3}(0) < 0.4$. Moreover, panel (b) of Fig. 5 also shows that the input polarization arrangement with elliptically polarized input pump and signal remains

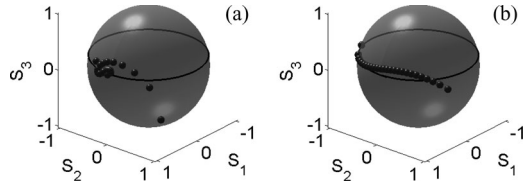

Fig. 6. Tips of the output vectors $\bar{\mathbf{S}}_{\mathbf{y}}^{(k)}$ for in-phase input excitation, pump and signal with input elliptical SOP, and $\bar{P}_{x3}(0) = 0.2$. Panel (a): $r = 1$ and $\xi = 8.5$; panel (b): $r = 3$ and $\xi = 1.8$. The black circle indicates the parallel $S_3 = 0.2$.

sensitive to the value of the power ratio $r = P/S$: indeed substantial modal attraction is only observed whenever $r > 0.8$.

From Fig. 5(b) it is also interesting to point out that, for in-phase input modal excitation, the peak DOMA values grow larger as r is increased, irrespective of the input pump MPD. Therefore in this case one may always improve the efficiency of modal attraction, albeit at the expense of higher pump powers. For example, with $r = 3$ the peak DOMA value is 0.93 at $\xi = 1.8$. The enhancement of the modal attraction strength as the relative pump/signal power is increased may also be observed in the plots of Fig. 6, where the output vector tips $\bar{\mathbf{S}}_{\mathbf{y}}^{(k)}$ are shown over the modal Poincaré sphere for an input pump MPD $\bar{P}_{x3}(0) \equiv \bar{P}_{y3}(0) = 0.2$. In Fig. 6(a) the pump/signal power ratio $r = 1$, whereas in Fig. 6(b) we set $r = 3$. Note that the output vectors shown in Fig. 6 correspond to the positions of maximum DOMA: hence $\xi_{\mathrm{peak},r=1} = 8.5$ in Fig. 6(a) and $\xi_{\mathrm{peak},r=3} = 1.8$ in Fig. 6(b), respectively. The panel (b) of Fig. 6 clearly shows that with $r = 3$ the alignement along the parallel $S_3 = 0.2$ is more uniform than with $r = 1$ (see panel (a)). Such enhancement of the modal attraction strength with larger pump/signal relative power values is not observed for out-of-phase input modal excitations: in this case, numerical simulations show that the DOMA values remain low even for $r \gg 1$ (not shown here).

Finally, let us consider the second input polarization arrangement presented in Section III, involving an input pump which is linearly polarized and aligned with one of the birefringence axes ($\mathbf{p_0}(0) \equiv \mathbf{p_1}(0) = [0, 0, \pm 1]$), and input signal with elliptical polarization ($\mathbf{s_0}(0) \equiv \mathbf{s_1}(0) = [s, t, 0]$). In this case, one still may obtain efficient modal attraction whenever $-0.4 < \bar{P}_{x3}(0) < 0.4$. In fact, Fig. 7(a) shows that, whenever

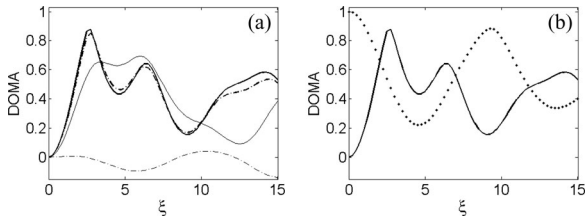

Fig. 7. Panel (a): Same as in Fig. 5, with linearly polarized pump aligned with one of the principal axes of the fiber. Panel (b): DOMAs of signal (bold line) and pump (dotted line) with $P_{x0} = S_{y0}$, in-phase input modal excitation, and $\bar{P}_{x3}(0) = 0$.

$P_{x0} = S_{y0}$ and for in-phase input modal excitation, peak values of DOMA $\simeq 0.9$ are obtained at $\xi_{\rm peak} = 2.8$. Similarly with the previously considered polarization configurations, the strength of modal attraction may be increased by making the pump/signal power ratio $r = P/S$ larger. Again, the condition of in-phase modal excitation is necessary for achieving high DOMA values.

Numerical solutions of (2), (3) (and the associated equations for $\mathbf{P}_y$ and $\mathbf{S}_x$) demonstrate an interesting property of the modal attraction process. Namely, similarly to what happens with polarization attraction, attraction of the the signal MPD $\bar{S}_{y3}$ toward the input pump MPD $\bar{P}_{x3}(0)$ is accompanied by a spreading of the pump MPD $\bar{P}_{x3}(z)$ between -1 and 1, irrespectively of the input SOP and the power ratio value r. If one computes the DOMA for the pump beam $\bar{\mathbf{P}}_{\mathbf{x}}$, one obtains that this value (which is initially equal to 1 at $\xi = 0$, since all occurences $\bar{P}^{(k)}_{x3}(0)$ are fixed to one and the same value) progressively decreases along the fiber until it reaches relatively low values. This property is clearly illustrated in Fig. 7(b), where we show the signal and pump DOMAs for the case with $r = 1$ and $\bar{P}_{x3}(0) = 0$ when the input pump is linearly polarized along the x axis and the input signal is elliptically polarized. As it can be seen, the DOMA associated with the pump reaches a minimum value of 0.22 at $\xi = 4.5$. Finally, we point out that results similar to the case of Fig. 7 are obtained whenever the input signal is linearly polarized along one of the principal birefringence axes ($\mathbf{s_0}(0) \equiv \mathbf{s_1}(0) = [0, 0, \pm 1]$), and the input pump has an elliptical SOP ($\mathbf{p_0}(0) \equiv \mathbf{p_1}(0) = [p, q, 0]$).

V. Conclusion

In this paper, we analyzed the polarization dependence of modal attraction, which is induced on a signal beam by a pump beam which copropagates in a bimodal birefringent fiber. Modal attraction means that the input power distribution of the x- (y-) polarized pump modes is reproduced by the y- (x-) polarized signal modes at a certain point along the fiber, nearly irrespectively of the signal input modal distribution. We extended the theoretical treatment that was developed in [11], where the two beams were supposed to be linearly and orthogonally polarized along the principal axes of the fiber, to the most general case where the pump and signal beams may posses an arbitrary input SOP. We have shown that the strength of modal attraction is sensitive to the input polarizations of pump and signal: more precisely, to the third component of the signal and pump SOPs.

In order to put in evidence the dependence of the modal attraction on the input polarizations of the beams, we focused on four different special configurations of the input SOPs, which exhibit different properties in the modal attraction process. In particular, each polarization arrangement requires a different value for the critical nonlinear intermodal coefficient $C = C_{01}$ which is necessary to achieve efficient modal attraction. We have designed a depressed index, double core fiber which is bimodal in the telecom band from 1520 to 1580 nm, and provides the necessary coupling coefficient C_{01} for ensuring strong modal attraction in each of the considered polarization arrangements.

We have also shown that the DOMA, as well as the point in the fiber where attraction is observed, both vary with the input polarization configuration. In any case, in-phase modal excitation is a necessary condition for obtaining significant modal attraction. Moreover, in this case the modal attraction strength can be enhanced by increasing the relative power of the pump beam with respect to the signal power. Finally, we observed that the attraction of the signal MPD toward the input pump modal distribution goes together with a spreading of the pump modal distribution upon propagation. Although possible in principle, extension of the analysis of modal attraction to the general case of a multimode optical fiber (even beyond the weakly guiding limit) appears to be challenging, since a careful design of the inter-modal coupling coefficients and dispersion characteristics is required for achieving a specific PM condition among the different propagating modes. We foresee that the effect of modal attraction has the potential for being exploited as a nonlinear mode converter for the ultrafast all-optical control of the spatial multiplexing of beams in multimode fiber optics transmission systems where signals are individually coupled over the modes, so that the in-phase modal condition can be achieved [6], [8], [14].

Appendix

We write the $a-$ polarized ($a = \{x, y\}$) CW incident field at the input of the fiber (z = 0) and at the pump frequency ω_p as $E_{{\rm tot},a}(x, y, \omega_p) = E_a G(x, y) \exp(i\omega_p t) + \text{c.c.}$ (c.c. means complex conjugate), where $G(x, y)$ is the transverse profile of the incident field and E_x, E_y are two complex values indicating its polarization. According to the usual decomposition of the input field over the spatial modes $M_n(x, y)$ of the fiber, the input amplitudes read as $U_{na}(0) = E_a I_n$, where $I_n = (\int_{xy} G(x, y) M^*_n(x, y) dxdy)/(\int_{xy} |M_n(x, y)|^2 dxdy)$. One thus immediately finds that the input component $p_{n1}(0) = (U_{nx}(0)U^*_{ny}(0) + c.c.)/(|U_{nx}(0)|^2 + |U_{ny}(0)|^2)$ of the polarization Stokes vector $\mathbf{p_n}(0)$ can be rewritten as $p_{01}(0) = p_{11}(0) = (E_x E^*_y + E^*_x E_y)/(|E_x|^2 + |E_y|^2)$. Whereas $p_{02}(0) = p_{12}(0)$ and $p_{03}(0) = p_{13}(0)$, hence $\mathbf{p_0}(0) = \mathbf{p_1}(0)$. Similarly we find that $\mathbf{s_0}(0) = \mathbf{s_1}(0)$.

Since $|U_{nx}(0)|^2 = p_{n0}(0)(1 + v_p)/2$ and $|U_{ny}(0)|^2 = p_{n0}(0)(1 - v_p)/2$, where $v_p = p_{n3}(0)$, and taking into account that $U_{0a}(0)U_{1a}(0)^* = |U_{0a}(0)U_{1a}(0)| \exp(i\phi_p)$, where ϕ_p is the relative phase between the amplitudes $U_{0a}(0)$ and $U_{1a}(0)$, it follows from the definition of the input unitary modal Stokes vectors that $\bar{\mathbf{P}}_{\mathbf{x}}(0) = \bar{\mathbf{P}}_{\mathbf{y}}(0) = \bar{\mathbf{P}}(0) = [\alpha_p \cos(\phi_p), -\alpha_p \sin(\phi_p), \nu_p]$, $\mathbf{P}_{\mathbf{x}}(0) =$

$(P/2)(1+v_p)\bar{\mathbf{P}}(0)$ and $\mathbf{P_y}(0) = (P/2)(1-v_p)\bar{\mathbf{P}}(0)$, where $\alpha_p = 2(p_{00}(0)p_{10}(0))^{1/2}/P$, $\nu_p = (p_{00}(0) - p_{10}(0))/P$ and $P = p_{00}(0) + p_{10}(0)$ is the total pump power. Similarly, one finds that $\bar{\mathbf{S}}_\mathbf{x}(0) = \bar{\mathbf{S}}_\mathbf{y}(0) = \bar{\mathbf{S}}(0) = [\alpha_s \cos(\phi_s), -\alpha_s \sin(\phi_s), \nu_s]$, $\mathbf{S_x}(0) = (S/2)(1+v_s)\bar{\mathbf{S}}(0)$ and $\mathbf{S_y}(0) = (S/2)(1-v_s)\bar{\mathbf{S}}(0)$: here v_s, α_s and ν_s are obtained from v_p, α_p and ν_p by interchanging U and V as well as P with S. Thanks to the invariance of the system of (2), (3) (and the associated equations for $\mathbf{P}_y$ and $\mathbf{S}_x$) to rotations of the input modal Stokes vectors about the third modal axis, one may rotate both $\bar{\mathbf{P}}(0)$ and $\bar{\mathbf{S}}(0)$ by the angle $-\phi_p$, which leads to same input modal Stokes vectors as they are reported in Section III.

REFERENCES

[1] D. Gloge, "Weakly guiding fibers," *Appl. Opt.*, vol. 10, pp. 2252–2258, 1971.

[2] S. J. Garth and C. Pask,"Nonlinear effects in elliptical-core few-mode optical fibers," *J. Opt. Soc. Amer. B*, vol. 9, pp. 243–250, 1992.

[3] S. J. Garth and R. A. Sammut,"Theory of stimulated Raman scattering in two-mode optical fibers," *J. Opt. Soc. Amer. B*, vol. 10, pp. 2040–2047, 1993.

[4] S. Pitois, A. Picozzi, G. Millot, H. R. Jauslin, and M. Haelterman, "Polarization and modal attractors in conservative counterpropagating four-wave interaction," *Europhys. Lett.*, vol. 70, pp. 88–94, 2005.

[5] R. Ryf, S. Randel, A. H. Gnauck, C. Bolle, A. Sierra, S. Mumtaz, M. Esmaeelpour, E. C. Burrows, R. Essiambre, P. J. Winzer, D. W. Peckham, A. H. McCurdy, and R. Lingle, "Mode-division multiplexing over 96 km of few-mode fiber using coherent 6 x 6 MIMO processing," *J. Lightwave Technol.*, vol. 30, no. 4, pp. 521–531, Feb. 2012.

[6] M. Salsi, C. Koebele, D. Sperti, P. Tran, H. Mardoyan, P. Brindel, S. Bigo, A. Boutin, F. Verluise, P. Sillard, M. Astruc, L. Provost, and G. Charlet, "Mode division multiplexing of 2 x 100Gb/s channels using an LCOS based spatial modulator," *J. Lightwave Technol.*, vol. 30, no. 4, pp. 618–623, Feb. 2012.

[7] A. Mecozzi, C. Antonelli, and M. Shtaif, "Nonlinear propagation in multimode fibers in the strong coupling regime," *Opt. Exp.*, vol. 20, pp. 11673–11678, 2012.

[8] S. Mumtaz, R. J. Essiambre, and G. P. Agrawal, "Nonlinear propagation in multimode and multicore fibers: Generalization of the Manakov equations," *J. Lightwave Technol.*, vol. 31, no. 3, pp. 398–406, Feb. 2013.

[9] V. V. Kozlov, K. Turitsyn, and S. Wabnitz, "Nonlinear repolarization in optical fibers: Polarization attraction with copropagating beams," *Opt. Lett.*, vol. 36, pp. 4050–4052, 2011.

[10] V. V. Kozlov, J. Nuño, and S. Wabnitz," Theory of lossless polarization attraction in telecommunication fibers," *J. Opt. Soc. Amer. B*, vol. 28, pp. 100–108, 2011.

[11] M. Guasoni, V. V. Kozlov, and S. Wabnitz, "Theory of modal attraction in bimodal birefringent fibers," *Opt. Lett.*, vol. 38, pp. 2029–2031, 2013.

[12] C. Antonelli, A. Mecozzi, M. Shtaif, and P. J. Winzer, "Stokes-space analysis of modal dispersion in fibers with multiple mode transmission," *Opt. Exp.*, vol. 20, pp. 11718–11733, 2013.

[13] C. Antonelli, A. Mecozzi, M. Shtaif, and P. J Winzer, "Random coupling between groups of degenerate fiber modes in mode multiplexed transmission," *Opt. Exp.*, vol. 21, pp. 9484–9490, 2013.

[14] P. Sillard, M. Bigot-Astruc, D. Boivin, H. Maerten, and L. Provost "Few-mode fiber for uncoupled mode-division multiplexing transmissions," presented at the 37th Eur. Conf. Exhib. Opt. Commun., Geneva, Switzerland, 2011, Paper Tu.5.7.

Authors' biographies not available at the time of publication.